ALMA reveals a candidate hot and compact disc around the O-type protostar IRAS 16547−4247

Luis A. Zapata,[1][*] Aina Palau,[1] Roberto Galván-Madrid,[1,2] Luis F. Rodríguez,[1] Guido Garay,[3] James M. Moran[4] and Ramiro Franco-Hernández[3]

[1]*Centro de Radiostronomía y Astrofísica, Universidad Nacional Autónoma de México, 58089 Morelia, Michoacán, México*
[2]*European Southern Observatory, Karl-Schwarzschild-Str. 2, D-85748 Garching, Germany*
[3]*Departamento de Astronomía, Universidad de Chile, Casilla 36-D, Santiago, Chile*
[4]*Harvard–Smithsonian Center for Astrophysics, 60 Garden Street, Cambridge, MA 02138, USA*

ABSTRACT

We present high angular resolution (∼0.3 arcsec) submillimeter continuum (0.85 mm) and line observations of the O-type protostar IRAS 16547−4247 carried out with the Atacama Large Millimeter/Submillimeter Array (ALMA). In the 0.85 mm continuum band, the observations revealed two compact sources (with a separation of 2 arcsec), one of them associated with IRAS 16547−4247, and the other one to the west. Both sources are well-resolved angularly, revealing a clumpy structure. On the other hand, the line observations revealed a rich variety of molecular species related to both continuum sources. In particular, we found a large number of S-bearing molecules, such as the rare molecule methyl mercaptan (CH_3SH). At scales larger than 10 000 au, molecules (e.g. SO_2 or OCS) mostly with low-excitation temperatures in the upper states ($E_k \lesssim 300$ K) are present in both millimeter continuum sources, and show a southeast–north-west velocity gradient of 7 km s^{-1} over 3 arcsec (165 km s^{-1} pc^{-1}). We suggest that this gradient probably is produced by the thermal (free–free) jet emerging from this object with a similar orientation at the base. At much smaller scales (about 1000 au), molecules with high-excitation temperatures ($E_k \gtrsim 500$ K) are tracing a rotating structure elongated perpendicular to the orientation of the thermal jet, which we interpret as a candidate disc surrounding IRAS 16547−4247. The dynamical mass corresponding to the velocity gradient of the candidate to disc is about 20 M$_\odot$, which is consistent with the bolometric luminosity of IRAS 16547−4247.

Key words: stars: protostars – ISM: jets and outflows.

1 INTRODUCTION

Recent theoretical studies by Krumholz et al. (2009), Peters et al. (2010), and Kuiper et al. (2010) have demonstrated that stars up to 140 M$_\odot$ can be formed in a similar way to the low- and intermediate-mass stars, that is, through flattened accretion discs. The existence of discs around high-mass stars solves the long-standing radiation pressure problem, where the powerful radiation pressure of the star is expected to halt the infalling material. However, at this point, there is a lack of detections of centrifugally supported circumstellar discs surrounding young O-type stars due probably to the large distances of the stars (a few kpc), their very small number, and the complexity of the regions of massive star formation (e.g. Zinnecker & Yorke 2007; Zapata et al. 2011; Naranjo-Romero et al. 2012).

There are a few cases where discs rotationally supported are present in young O-type stars associated with a large luminosity (of about 10$^{4-5}$ L$_\odot$): AFGL2591-VLA3, Wang, van der Tak & Hogerheijde (2012), Jiménez-Serra et al. (2012); IRAS 18360−0537, Qiu et al. (2012); NGC 7538 IRS1, Moscadelli & Goddi (2014); Klaassen et al. (2009); Hoffman (2012); W51 North, Zapata et al. (2009), Zapata, Tang & Leurini (2010); W33A, Galván-Madrid et al. (2010). In the cases of IRAS 18360−0537, NGC 7538 IRS1, and W51 North, there is some evidence that the innermost parts of the discs are Keplerian, similar to the rotating structures found in low-mass stars. It is important to note that most of these structures are ≳5000 au in size (with the exception of AFGL 2591 and NGC 7538), and most likely are forming systems of massive stars.

IRAS 16547−4247 (hereafter IRAS 16457) is catalogued as a young massive protostar with a bolometric luminosity of 6.2 × 10^4 L$_\odot$ (Garay et al. 2003), equivalent to that of a single O8 zero-age main-sequence star (Panagia 1973), although it is

[*]E-mail: lzapata@crya.unam.mx

probably a cluster for which the most massive source would have a slightly lower luminosity. The source is located at a distance of 2.9 ± 0.6 kpc (Rodríguez et al. 2008). Observations at radio wavelengths have revealed a triple continuum source that is aligned in a north-west–south-east (NW–SE) direction (position angle: P.A. $\sim 140°$), with the outer lobes symmetrically separated from the central source by an angular distance of ~ 10 arcsec , equivalent to a physical separation in the plane of the sky of ~ 0.14 pc (Garay et al. 2003). The fit to the radio jet by Rodríguez et al. (2008) gives a position angle of $137°$ within a few arcseconds from the star. It should be noted however that at smaller scales the core of the jet shows a somewhat different position angle of $164°$ (Rodríguez et al. 2008). In this paper, we will adopt as the representative position angle of the jet the value of $137°$.

The central source – related to the infrared source IRAS 16547 – has a positive spectral index which is consistent with that expected for a radio thermal (free–free) jet, while the spectral index of the lobes suggests a mix of thermal and non-thermal emission (Araudo et al. 2007). The APEX molecular observations of Garay et al. (2007) revealed the presence of a massive and energetic bipolar outflow (flow mass $\sim 110\,M_\odot$; mass outflow rate $\sim 10^{-2}\,M_\odot\,\mathrm{yr}^{-1}$; momentum $\sim 10^3\,M_\odot\,\mathrm{km\,s}^{-1}$; and kinetic energy 10^{48} erg) with lobes ~ 0.7 pc in extent and aligned with the thermal jet located at the centre of the core.

Very Large Array (VLA) and Submillimeter Array (SMA) observations with high spatial resolution have revealed a rotating structure associated with IRAS 16547, traced at small scales (~ 50 au) by the H_2O masers and at moderate scales (~ 1000 au) by the thermal emission of SO_2. However, both rotating structures have slightly different position angles and most likely are tracing different parts of IRAS 16547. The SO_2 rotating structure has an east–west orientation (P.A. $\sim 90°$), while the H_2O structure a P.A. $\sim 40°$. The poorly resolved structure of the SO_2 can be modelled as a rotating ring or two separate objects, while the H_2O rotating structure, on the other hand, was suggested to be a compact Keplerian disc surrounding IRAS 16547 (Franco-Hernández et al. 2009).

In this study, we present submillimeter line and continuum observations, made with the Atacama Large Millimeter/Submillimeter Array (ALMA) of the massive protostar IRAS 16547. We report on the detection of a candidate to compact and hot molecular rotating disc with a size of about 1000 au and with an orientation perpendicular to the radio jet emerging from this object. In Sections 2 and 3, we discuss the observations and results. In Section 4, we present the discussion and conclusions.

2 OBSERVATIONS

The observations were carried out with 32 antennas of ALMA on 2012 April (16 antennas) and August (21 antennas), during the cycle 0 science data programme. The array at that point only included antennas with diameters of 12 m. The 496 independent baselines ranged in projected length from 25 to 364 m.

The phase reference centre for the observations was at $\alpha_{\mathrm{J2000.0}} = 16^\mathrm{h}58^\mathrm{m}17\overset{s}{.}24$, $\delta_{\mathrm{J2000.0}} = -42°52'08\overset{''}{.}09$, the position of the object IRAS 16547. The primary beam of ALMA at 345 GHz has an FWHM ~ 17.6 arcsec. The dusty emission from IRAS 16547 falls well inside of the full width at half-maximum (FWHM). The ALMA digital correlator was configured in four spectral windows of 1875 MHz and 3840 channels each. This provides a spectral resolution of 0.488 MHz ($\sim 0.4\,\mathrm{km\,s}^{-1}$) per channel. The spectral windows were centred at 350.355, 352.228, 340.117, and 341.971 GHz, in order to detect different spectral lines as for example, SO, ^{34}SO,

and CS. These lines had already been reported towards this massive young stellar object using the single dish telescopes SEST and APEX (Garay et al. 2003, 2007).

Observations of Titan provided the absolute scale for the flux density calibration. For the time-dependent gain calibration, the nearby quasar J0607−085 was observed approximately every 15 min. The quasar 3C 279 was used for the bandpass calibration.

The data were calibrated, imaged, and analysed using the Common Astronomy Software Applications (McMullin et al. 2007). To analyse the data, we also used the KARMA (Gooch 1996) and AIPS of the National Radio Astronomy Observatory (NRAO) software. In order to construct the continuum image, we used the total bandwidth of the observations (7.5 GHz) selecting only the line-free channels. However, as there are many lines detected in the spectral windows, we have probably some contamination from very faint lines. We used uniform weighting in the continuum and lines maps presented in this study. The resulting rms noise for the continuum image was 7 mJy beam^{-1} at an angular resolution of $0\overset{''}{.}39$ arcsec $\times$ $0\overset{''}{.}34$ arcsec with a P.A. $= 69\overset{\circ}{.}2$. For the line emission, the resulting rms noise was about 35 mJy beam^{-1} km s^{-1} at the same angular resolution.

3 RESULTS

3.1 0.85 mm continuum emission

In Fig. 1, we present the main results of the ALMA 0.85 mm continuum observations of IRAS 16547. The submillimeter source reported by Garay et al. (2003) was found to have a western extension by Franco-Hernández et al. (2009). We resolved the source into two continuum sources with a clumpy morphology, one of them associated with the infrared source IRAS 16547, and the other one 2 arcsec to its west (IRAS 16547-W). IRAS 16547-W was already reported by Franco-Hernández et al. (2009), and we find that its peak lies ~ 0.4 arcsec to the west of the centimetre source IRAS 16547 D (Rodríguez et al. 2008).

The continuum source associated with IRAS 16547 is at a position of $\alpha_{\mathrm{J2000.0}} = 16^\mathrm{h}58^\mathrm{m}17\overset{s}{.}211$, $\delta_{\mathrm{J2000.0}} = -42°52'07\overset{''}{.}47$. For IRAS 16547-W, it is difficult to obtain a position because of its extended clumpy morphology. The central position of IRAS 16547-W is $\alpha_{\mathrm{J2000.0}} = 16^\mathrm{h}58^\mathrm{m}17\overset{s}{.}051$, $\delta_{\mathrm{J2000.0}} = -42°52'07\overset{''}{.}11$. Using a Gaussian fitting, we found for IRAS 16547 a flux density and peak intensity values of 2.1 ± 0.1 Jy and 675 ± 30 mJy beam^{-1}, respectively. The Gaussian fitting was only made in the most central part of IRAS 16547, we do not include the SE–NW extended emission.

For IRAS 16547-W, we found a flux density and peak intensity values of 1.6 ± 0.20 Jy and 140 ± 30 mJy beam^{-1}, respectively. We also find from these fits that the IRAS 16547 source has a deconvolved size of $0\overset{''}{.}56 \pm 0\overset{''}{.}02$ arcsec $\times$ $0\overset{''}{.}50 \pm 0\overset{''}{.}02$ arcsec with a P.A. $= +115° \pm 5°$. Therefore, at the distance of this object (2.9 kpc), the size of the continuum source is about 1620 au $\times$ 1450 au.

Assuming that the dust is optically thin and isothermal, and following Hildebrand (1983), the dust mass (M_d) will be directly proportional to the flux density (S_ν) as

$$M = \frac{S_\nu D^2}{B_\nu(T_\mathrm{d})\kappa_\nu},\tag{1}$$

where S_ν is the flux density at the frequency ν, D is the distance to the Sun, $B_\nu(T_\mathrm{d})$ is the Planck function at the dust temperature T_d, and κ_ν is the absorption coefficient per unit of total (gas+dust)
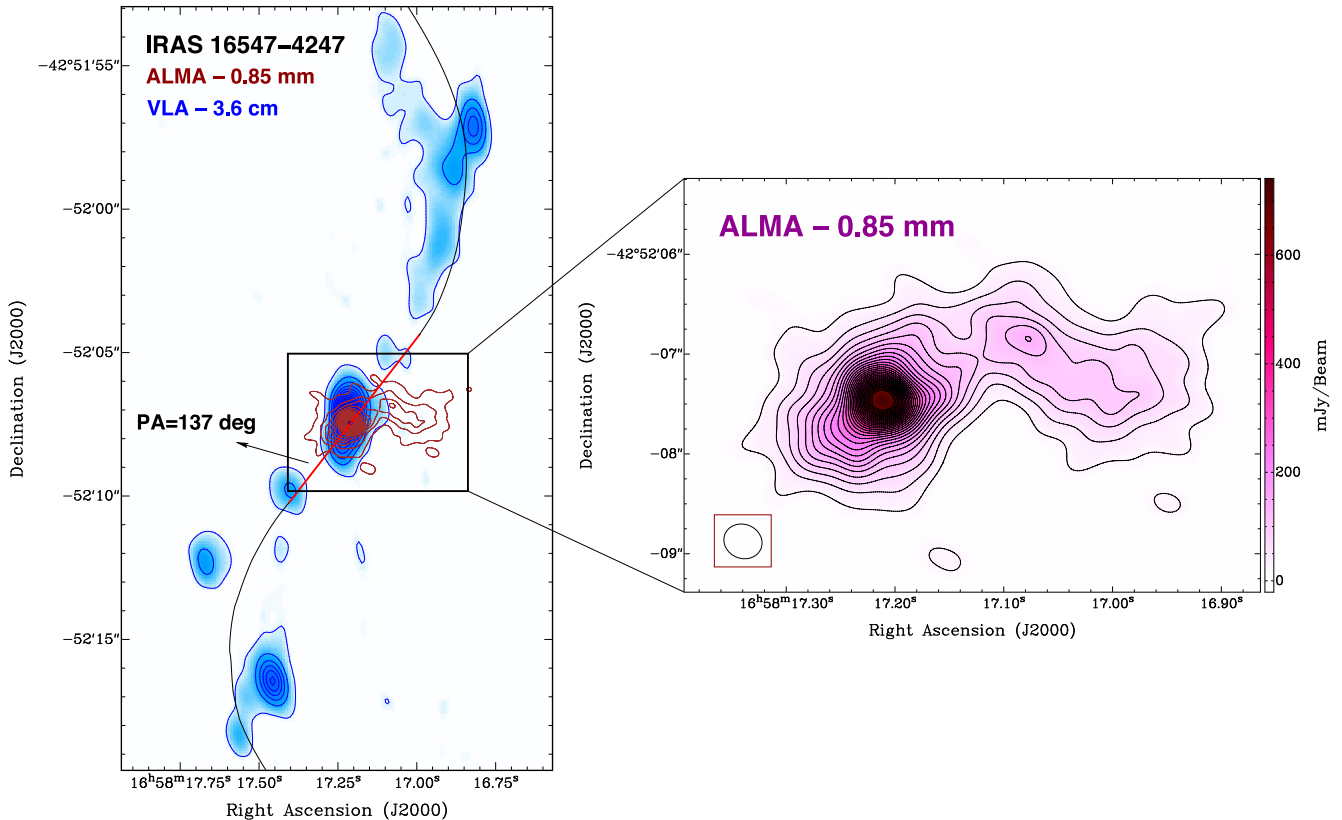
Figure 1. 3.6 cm and 0.85 mm continuum colour-scale/contours images from IRAS 16547 obtained with the VLA (Rodríguez et al. 2008) and The ALMA (this work), respectively. The blue colour-scale/contours show the continuum emission arising at 3.6 cm, while the violet colour-scale/contours show the continuum emission at 0.85 mm. Note that the 3.6 cm continuum emission traces a radio thermal (free–free) jet with an orientation NW–SE (Garay et al. 2003; Rodríguez et al. 2008), while the emission detected by ALMA is only present in the middle and traces dust thermal emission. The blue contours range from 5 to 90 per cent of the peak emission, in steps of 5 per cent. The peak of the centimetre continuum emission is 6 mJy beam^{-1}. The brown contours range from 5 to 90 per cent of the peak emission, in steps of 5 per cent. The violet contours (on the right panel) range from 6 to 90 per cent of the peak emission, in steps of 3 per cent. The peak of the millimeter continuum emission is 0.67 Jy beam^{-1}. The synthesized beam of the ALMA continuum image is shown in the lower-left corner, in the right image. The colour-scale bar on the right-hand panel indicates the peak flux in mJy beam^{-1}. The P.A. of the radio thermal jet close to the source is estimated to be around 137°, and the antisymmetric lines shows the jet trajectory associated with a precessing source model (Rodríguez et al. 2008). The rms noise for the ALMA continuum image is 7 mJy beam^{-1}.

mass density. Writing equation (1) in practical units (Palau et al. 2013):

$$\left[\frac{M}{M_\odot}\right] = 3.25 \times \frac{e^{0.048\,\nu/T_d} - 1}{\nu^3 \kappa_\nu} \times \left[\frac{S_\nu}{\text{Jy}}\right] \left[\frac{D}{\text{pc}}\right]^2, \qquad (2)$$

where T_d is in K, ν is in GHz, and κ_ν is in cm^2 g^{-1}. Taking a gas-to-dust ratio of 100, a distance of 2.9 kpc, a dust temperature of 250 K (Hernández-Hernández et al. 2014) for IRAS 16547 and 150 K (this value is uncertain and is obtained more or less from the excitation temperatures of some the lines present in this object) for IRAS 16547-W, and a dust mass opacity $\kappa_{850\,\mu\text{m}} = 0.015$ cm^2 g^{-1} (taking into account the gas-to-dust ratio; Ossenkopf & Henning 1994). We estimate the total mass associated with the dust continuum emission related to the disc in IRAS 16547 of 6.0 M$_\odot$ (integrating in an area ∼1 arcsec), and for IRAS 16547-W a mass of 8.0 M$_\odot$. The values of the masses obtained here for IRAS 16547 and IRAS 16547-W have uncertainties of at least a factor of 2, due mainly to the error in the determination to the dust mass opacity coefficient at this wavelength.

3.2 Line thermal emission

In Table 1, we show all spectral lines detected in these observations. We detected 15 molecular species with different transitions and their isotopologues. In particular, we found a large number of S-bearing molecules, for example the rare molecule methyl mercaptan (CH$_3$SH). This molecule has been detected only in two star-forming regions (G327 and B1; Gibb et al. 2000; Cernicharo et al. 2012), other than the Galatic Center (Linke, Frerking & Thaddeus 1979) and Orion-KL (Kolesniková et al. 2014), and is supposed to trace hot regions were desorption from grain mantles is very efficient (Cernicharo et al. 2012).

In order to properly identify the lines detected in the four ALMA spectral windows, we built synthetic spectra for all the possible molecules with transitions within ±3 MHz of a given line, and compared the synthetic spectra with the observed spectra in the four observed windows, see Fig. 2 and Table 1. This allowed us to take into account blending and contributions from transitions of different molecules to a given line. The synthetic spectra were computed assuming local thermodynamic equilibrium and optically thin emission as in Palau et al. (2011), and using the molecular data from the Jet Propulsion Laboratory (Pickett et al. 1998) and the

Table 1. Transitions detected towards IRAS 16547.

Molecule	Transition	Rest freq. (GHz)	$S_{ij}{}^a\mu^2$ (D^2)	E_u (K)
SO_2 $v=0$	$18_{4,\,14}-18_{3,\,15}$	338.305 99	26.81	197
	$20_{1,\,19}-19_{2,\,18}$	338.611 81	26.02	199
	$28_{2,\,26}-28_{1,\,27}$	340.316 41	32.05	392
	$5_{3,\,3}-4_{2,\,2}$	351.257 22	7.32	36
SO_2 $v_2=1$	$4_{3,\,1}-3_{2,\,2}$	338.348 74	7.07	792
	$8_{2,\,6}-7_{1,\,7}$	338.376 38	5.09	803
$^{34}SO_2$ $v=0$	$13_{2,\,12}-12_{1,\,11}$	338.320 36	13.59	93
$^{33}SO_2$ $v=0$	$8_{4,\,4}-8_{3,\,5}$, $F=19/2-19/2$	351.177 96	11.16	73
	$9_{4,\,6}-9_{3,\,7}$, $F=21/2-21/2$	351.281 37	12.88	81
	$19_{4,\,16}-19_{3,\,17}$, $F=41/2-41/2$	353.741 56	25.37	217
$SO^{18}O$	$20_{0,\,20}-19_{1,\,19}$	338.638 82	43.41	184
OCS	28–27	340.449 27	14.32	237
HNCS a-type	$30_{1,\,30}-29_{1,\,29}$	351.227 43	80.60	324
$SO^{17}O$	$20_{1,\,20}-19_{0,\,19}$	353.625 33	263.56	186
CH_3SH	$14_{13}-13_{13}$ $-/+A$	353.417 36	3.32	864
	$14_{13}-13_{13}$ E	353.431 07	3.33	863
	14_9-13_9 $-/+A$	353.672 82	14.10	479
	14_2-13_2 $-A$	353.726 26	23.60	147
	14_8-13_8 $-/+A$	353.734 46	16.20	406
	14_8-13_8 E	353.741 53	16.27	408
	14_7-13_7 E	353.777 78	18.11	341
	$14_{-7}-13_{-7}$ E	353.780 50	18.11	342
CH_3OH	$7_{-1,\,7}-6_{-1,\,6}$	338.344 63	5.54	71
	$7_{0,\,7}-6_{0,\,6}$ $++$	338.408 68	5.66	65
	$7_{-6,\,1}-6_{-6,\,0}$	338.430 93	1.50	254
	$7_{6,\,1}-6_{6,\,0}$ $++$	338.442 34	1.49	259
	$7_{-5,\,2}-6_{5,\,1}$	338.456 50	2.76	189
	$7_{5,\,3}-6_{5,\,2}$	338.475 29	2.76	201
	$7_{5,\,3}-6_{5,\,2}$ $++$	338.486 34	2.77	203
	$7_{2,\,6}-6_{2,\,5}$ $--$	338.512 86	5.23	103
	$7_{4,\,3}-6_{4,\,2}$	338.530 25	3.82	161
	$7_{3,\,5}-6_{3,\,4}$ $++$	338.540 80	4.60	115
	$7_{-3,\,5}-6_{-3,\,4}$	338.559 93	4.64	128
	$7_{3,\,4}-6_{3,\,3}$	338.583 19	4.62	113
	$7_{1,\,6}-6_{1,\,5}$	338.615 00	5.68	86
	$7_{2,\,5}-6_{2,\,4}$ $++$	338.639 94	5.23	103
	$7_{2,\,5}-6_{2,\,4}$	338.721 63	5.14	87
	$7_{-2,\,6}-6_{-2,\,5}$	338.722 94	5.20	91
	$16_{6,\,10}-17_{5,\,13}$ $++$	340.393 67	3.57	509
CH_3CH_2OH	$15_{7,\,8}-15_{6,\,9}$	338.886 21	13.67	162
CN $v=0$	$N=3-2$, $J=7/2-5/2$, $F=9/2-7/2$	340.247 77	9.01	33
	$N=3-2$, $J=7/2-5/2$, $F=5/2-5/2$	340.261 77	0.59	33
	$N=3-2$, $J=7/2-5/2$, $F=7/2-7/2$	340.264 95	0.58	33
CH_2NH	$3_{1,\,3}-2_{0,\,2}$, $F=4-3$	340.354 31	6.07	26
NH_2CHO	$16_{3,\,14}-15_{3,\,13}$	340.491 09	605.53	166
HNCO $v=0$	$16_{4,\,13}-15_{4,\,12}$	351.240 85	30.93	794
$H_2{}^{13}CO$	$5_{0,\,5}-4_{0,\,4}$	353.811 87	27.17	51
H_2CCNH	$11_{2,\,10}-12_{1,\,12}$	353.389 12	4.25	97
CH_3CHO^b	$19_{0,\,19}-18_{0,\,18}$ E	353.387 28	239.52	172
	$19_{0,\,19}-18_{0,\,18}$ A	353.425 95	239.30	172
CH_3OCHO $v=0^b$	$29_{4,\,25}-28_{4,\,24}$ E	353.401 85	74.20	274
CH_3OCHO $v=0^2$	$29_{4,\,25}-28_{4,\,24}$ A	353.410 59	74.21	274
CH_3OCHO $v=1^2$	$28_{7,\,21}-27_{7,\,20}$ A	353.575 58	69.94	461
CH_3OCHO $v=0^2$	$32_{2,\,31}-31_{2,\,30}$ E	353.723 60	84.18	290
CH_3OCHO $v=0^2$	$32_{2,\,31}-31_{2,\,30}$ A	353.728 62	84.15	290
CO^+	$J=3-2$, $F=5/2-3/2$	353.741 26	2.40	34

^{a}Line strength as given by the *Splatalogue*.
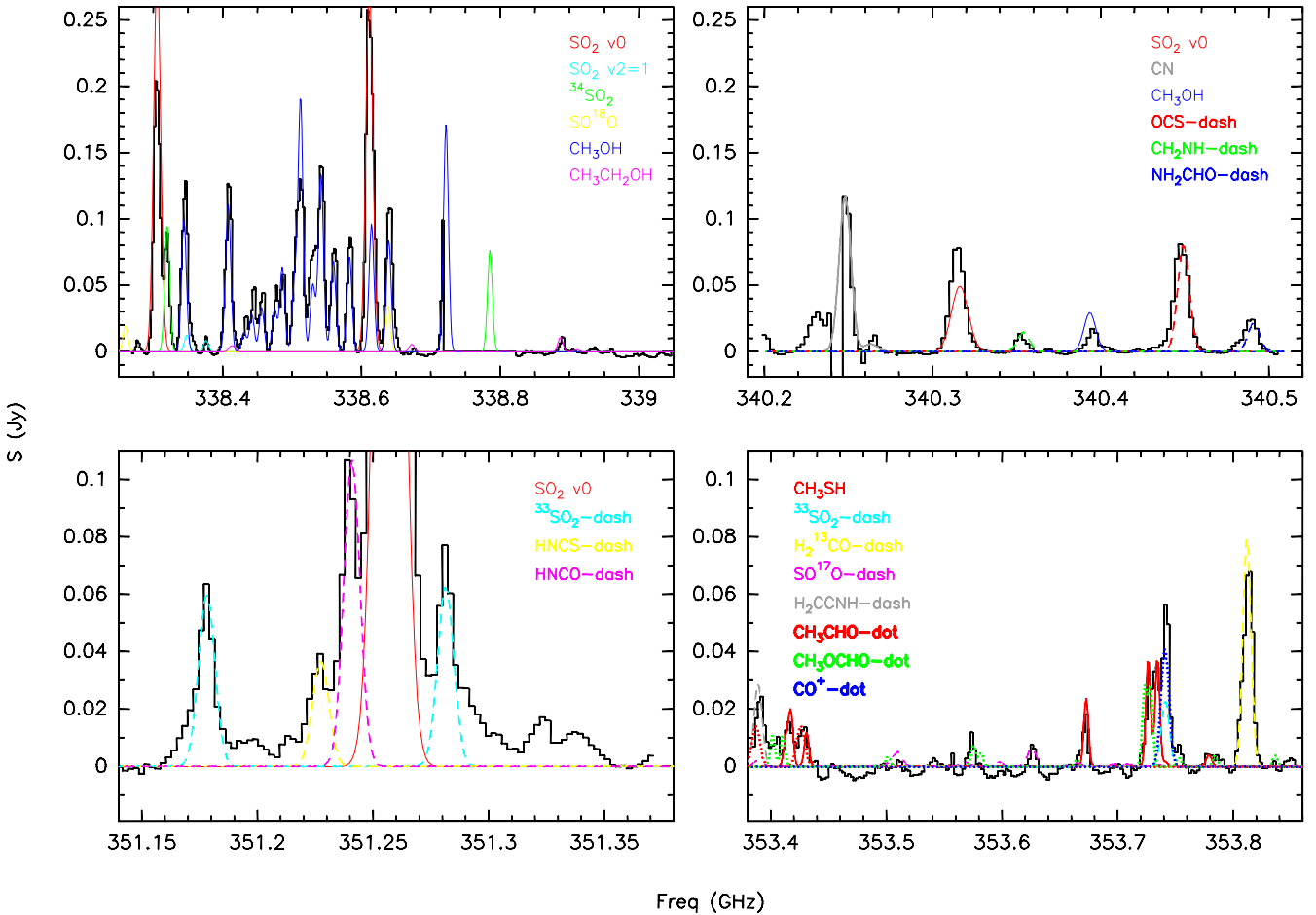^{b}Marginal/blended detections.

Figure 2. Average ALMA spectra obtained from IRAS 16547. The colour lines represent the synthetic LTE spectra assuming the parameters described in the text. We remark that this synthetic spectra in only used for line identification.

Cologne Database for Molecular Spectroscopy (Müller et al. 2005). Frequencies and energy levels of methyl mercaptan were taken from the Spectral Line Atlas of Interstellar Molecules (SLAIM, the catalogue of Frank Lovas, accessible only through Splatalogue[1]). To build the synthetic spectra, we adopted a linewidth (FWHM) of 7 km s^{-1} (except for the SO$_2$ lines, for which we used a linewidth of 10 km s^{-1}), and used rotational temperatures in the range 70–300 K (Hernández-Hernández et al. 2014). We then varied the column density until the synthetic spectra reasonably matched the observed spectra.

In Fig. 3, we show the first moment or the intensity weighted velocity of the SO$_2$ $v=0$ $28_{2,26}$–$28_{1,27}$ and OCS (28–27) thermal emission. Emission from these two molecules is present in IRAS 16547 as well as IRAS 16547-W. Both molecules emit at similar systemic local standard of rest (LSR) velocities. The LSR systemic velocity of IRAS 16547 is −30.6 km s^{-1} (Garay et al. 2003). In both molecules, the thermal emission associated with IRAS 16547 is stronger and more compact than that present in IRAS 16547-W. IRAS 16547 shows a clear velocity gradient of 7 km s^{-1} over a distance of 3 arcsec (equivalent to 165 km s^{-1} pc^{-1}). Franco-Hernández et al. (2009) also reported the detection of the SO$_2$ at 1 mm in IRAS 16547 with a smaller velocity gradient (2 km s^{-1} over

3 arcsec or 47.6 km s^{-1} pc^{-1}) at similar scales. This small velocity gradient is probably caused by the lower sensitivity of the SMA compared to ALMA. Convolving the ALMA SO$_2$ map to the angular resolution reported in Franco-Hernández et al. (2009) revealed similar results. We also noted that the SO$_2$ line mapped in SMA study has an excitation energy much higher than that observed by Franco-Hernández et al. (2009, 118 K). The blueshifted gas emission is located to its SE, while the redshifted gas velocities is at its NW. In these new ALMA observations, the velocity gradient is seen in both molecules (SO$_2$ and OCS), with some redshifted gas associated with IRAS 16547-W.

The first moment or the intensity weighted velocity of the CH$_3$SH 14_9-13_9 −/+A and CH$_3$OH $16_{6,10}$−$17_{5,13}$ ++ thermal emission is presented in Fig. 4. The emission from these two molecules is exclusively present in IRAS 16547, and is resolved with dimensions of 05 arcsec × 03 arcsec with a P.A. = 40°, corresponding to 1450 au × 870 au. There is a clear velocity gradient in both molecules and with an orientation almost perpendicular to that of the thermal jet and the molecules SO$_2$ and OCS. The blueshifted gas emission is found to its NE, while the redshifted is at its SW.

The kinematics of the gas emission traced by the molecules CH$_3$SH 14_9–13_9 −/+A and CH$_3$OH $16_{6,10}$−$17_{5,13}$ ++ is presented in the Fig. 5. The position angle where this diagram was computed is 40°. This reveals more clearly the velocity gradient observed in Fig. 4 with a magnitude of 8 km s^{-1} over 1 arcsec
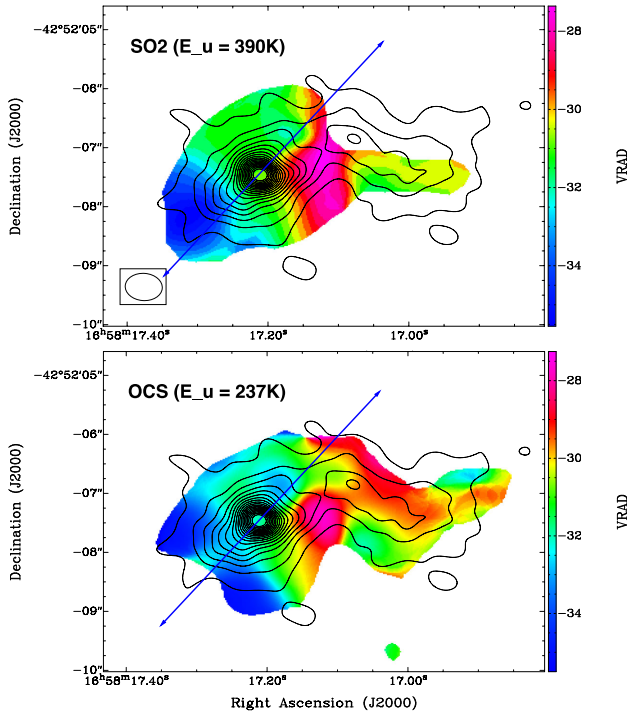
Figure 3. SO_2 $v=0$ $28_{2,26}-28_{1,27}$ and OCS (28–27) thermal emission integrated-intensity weighted velocity (moment one) colour maps overlaid with the 0.85 mm continuum maps from IRAS 16547. The black contours show the continuum emission arising at 0.85 mm. The contours range from 5 to 90 per cent of the peak emission, in steps of 5 per cent. The peak of the millimeter continuum emission is 0.67 Jy beam^{-1}. The synthesized beam of the ALMA continuum image is shown in the lower-left corner of the upper panel. The colour-scale bar on the right indicates the LSR radial velocities in km s^{-1}. The LSR systemic velocity of IRAS 16547 is -30.6 km s^{-1} (Garay et al. 2003). The blue line in both panels marks the orientation of the thermal (free–free) jet (Garay et al. 2003; Rodríguez et al. 2008) with a P.A. estimated to be around $137°$.

(equivalent to 566 km s^{-1} pc^{-1}). A small contribution of Keplerian velocities is observed to the NE of the source. The reason why we do not see the full Keplerian motions in this position–velocity diagram is probably because we need to better resolve the innermost parts of the possible disc, where the velocities increment more rapidly. However, there is also the possibility that the motions of the innermost parts of the disc are intrinsically non-Keplerian.

4 DISCUSSION

The ALMA observations towards IRAS 16547 revealed a rich variety of molecular species related to both continuum sources (see Table 1). This molecular emission is present at different scales and temperatures. The molecules presented in Fig. 3 (SO_2 or OCS) trace, at scales about 10^4 au, a clear velocity gradient with a similar orientation to the thermal jet. Some other molecules also detected in this observation (e.g. CH_3OH, CH_2NH, H_2CCNH) with similar excitation temperatures in the upper states ($E_u \sim 300$ K) are tracing similar structures at scales of some 10^4 au. On the other hand, the maximum velocity that an object with mass m can achieve under a gravitational field of an object with mass M
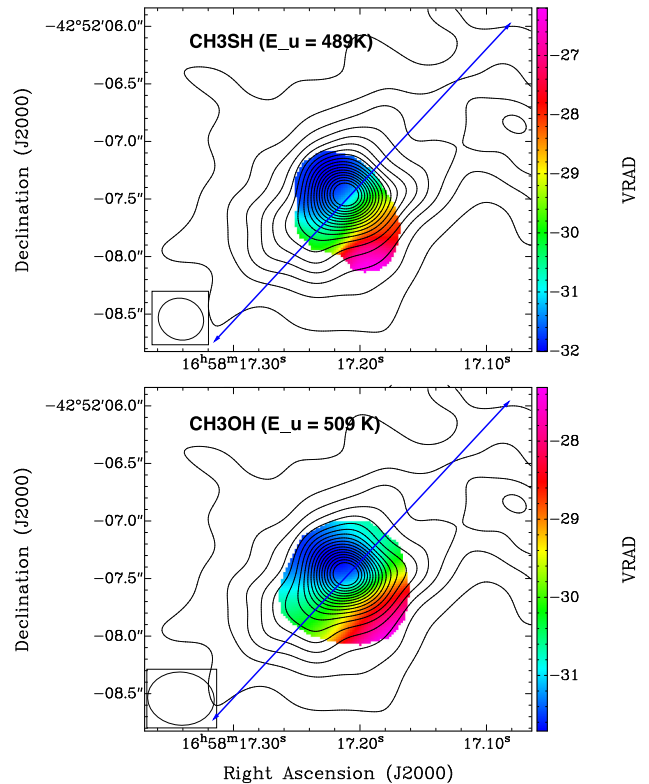

Figure 4. CH_3SH 14_9-13_9 $-/+A$ and CH_3OH $16_{6,10}-17_{5,13}$ $++$ integrated-intensity weighted velocity (first moments) colour maps overlaid with the 0.85 mm continuum maps from the innermost parts of IRAS 16547. The black contours show the continuum emission arising at 0.85 mm. The contours range from 5 to 90 per cent of the peak emission, in steps of 5 per cent. The peak of the millimeter continuum emission is 0.67 Jy beam^{-1}. The synthesized beam of the ALMA continuum image is shown in the lower-left corner. The colour-scale bar on the right indicates the LSR radial velocities in km s^{-1}. The LSR systemic velocity of IRAS 16547 is -30.6 km s^{-1} (Garay et al. 2003). The blue line in both panels, marks the orientation of the thermal (free–free) jet (Garay et al. 2003; Rodríguez et al. 2008) with a P.A. estimated to be around $137°$. The border of the velocity map corresponds to 3σ level.

can be inferred from a balance between gravity and centrifugal forces:

$$\frac{mv^2}{R} - \frac{GMm}{R^2} = 0,$$

where R is the distance to the object of mass M creating the gravitational field, G is the gravitational constant, and v is the velocity. This yields a dynamical mass given by

$$M = \frac{Rv^2}{G}.$$

Writing this equation in practical units, we obtain

$$M[\mathrm{M}_\odot] = 1.13 \times 10^{-3} \, v^2 \, [\mathrm{km \, s^{-1}}] \, R[\mathrm{au}].$$

If we assume that the gradient observed in Fig. 3 is produced by a rotating structure centred in IRAS 16547, we estimated a dynamical mass of $60 \, \mathrm{M}_\odot$. This mass corresponds to an early O-type protostar with a bolometric luminosity of $\sim 10^6 \, \mathrm{L}_\odot$ (Panagia 1973), which exceeds by one order of magnitude the bolometric luminosity of IRAS 16547 ($\sim 10^5 \, \mathrm{L}_\odot$). We then suggest that this gradient might be produced by the thermal jet that entrains the molecular gas, and
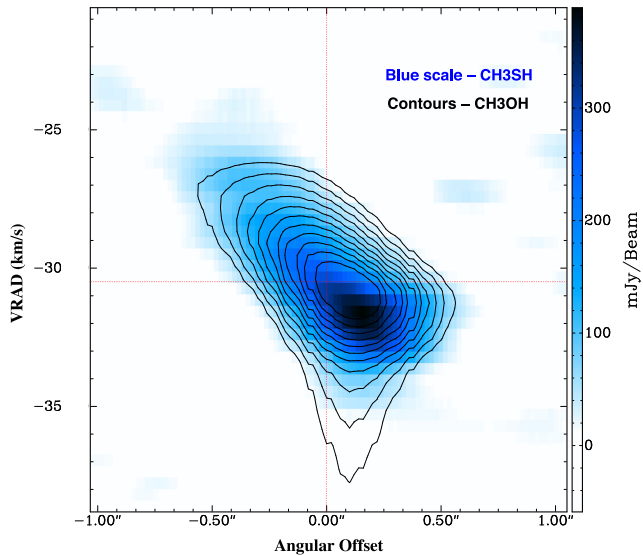
Figure 5. Position–velocity diagrams of the CH_3SH 14_9–13_9 $-/+A$ (blue scale) and CH_3OH $16_{6, 10}$–$17_{5, 13}$ $++$ (contours) emissions from the innermost parts of IRAS 16547. The contours range from 40 to 90 per cent of the peak emission, in steps of 5 per cent. The peak of the CH_3OH emission is 1.01 Jy beam^{-1}. The colour-scale bar on the right indicates the peak flux in mJy beam^{-1}. The LSR systemic velocity of IRAS 16547 is around -30.6 km s^{-1} (Garay et al. 2003). The spectral and angular resolutions are described in the text. The P.A. for both PV-diagrams (CH_3SH and CH_3OH) about $40°$. The units of the y-axis is in km s^{-1}. The angular offset here is relative to the peak of the continuum emission. The positive offsets are measured towards the NE. The 1σ rms level corresponds to 35 mJy beam^{-1}. The radial velocity here is LSR.

that has a similar orientation. Moreover, the emission of the high-velocity wings from the SO_2 is very extended in the direction of the jet. We therefore conclude that the SO_2 emission is most likely tracing an outflow.

At much more smaller scales ($\sim$1000 au), molecules with high-excitation temperatures ($E_u \gtrsim 500$ K) trace a compact rotating structure perpendicular to the orientation of the thermal jet (see Figs 4 and 5). This group of molecules includes: SO_2 $v_2 = 1$, HNCO $v=0$, CH_3SH, CH_3OH, etc. If we do a similar estimation as above, we obtain a dynamical mass of $\sim$26 M$_\odot$.This value for the mass is uncorrected by the inclination angle. This corresponds to a bolometric luminosity of 10^{4-5} L$_\odot$, a similar bolometric luminosity to that of IRAS 16547. Given the dimensions, the orientation, and the dynamical mass estimated from the velocity gradient traced by these molecules, we suggest that all these molecules trace a rotating disc surrounding IRAS 16547. Similar results are found for the dynamical mass of the protostar, if we assume that the water masers reported by Franco-Hernández et al. (2009) trace a very compact disc with a similar P.A., and at much more smaller scales ($\lesssim$300 au). An upper limit mass to the disc is $\sim$6 M$_\odot$, as estimated from the dust thermal emission. In conclusion, removing the mass of the disc, the protostar in the middle has a mass of $\sim$20 M$_\odot$.

It is interesting to note that even the same molecular species, but in different transitions (e.g. SO_2 and SO_2 v_2=1) trace distinct components of IRAS 16547. For example, the SO_2 v=0 $28_{2, 26}$–$28_{1, 27}$ is tracing the outflow (see Fig. 3), while the SO_2 v_2=1 $8_{2, 6}$–$7_{1, 7}$ is tracing the hot disc. This is because of the different excitation temperatures of the molecule at different transitions (see Table 1).

5 CONCLUSIONS

We have carried out submillimeter line and continuum observations made with ALMA of the massive protostar IRAS 16547. The main conclusions of this study are as follows.

(i) In the 0.85 mm continuum band, the observations revealed two compact sources (with a separation of $\sim$2 arcsec), one of them associated with IRAS 16547$-$4247, and the other one to the west. Both sources are well-resolved angularly, revealing a clumpy structure.

(ii) At scales larger than 10 000 au, molecules (e.g. SO_2 or OCS) mostly with low-excitation temperatures in the upper states ($E_k \lesssim 300$ K) are present in both millimeter continuum sources, and show a SE–NW velocity gradient of 7 km s^{-1} over 3 arcsec (165 km s^{-1} pc^{-1}). We suggest that this gradient probably is produced by the thermal (free–free) jet emerging from this object with a similar orientation at the base.

(iii) At much smaller scales (about 1000 au), molecules with high-excitation temperatures ($E_k \gtrsim 500$ K) are tracing a rotating structure elongated perpendicular to the orientation of the thermal jet, which we interpret as a candidate rotating disc surrounding IRAS 16547$-$4247. From Keplerian arguments, we estimate a mass of about 20 M$_\odot$ for the central star.

REFERENCES

Araudo A. T., Romero G. E., Bosch-Ramon V., Paredes J. M., 2007, A&A, 476, 1289
Cernicharo J., Marcelino N., Roueff E., Gerin M., Jiménez-Escobar A., Muñoz Caro G. M., 2012, ApJ, 759, L43
Franco-Hernández R., Moran J. M., Rodríguez L. F., Garay G., 2009, ApJ, 701, 974
Galván-Madrid R., Zhang Q., Keto E., Ho P. T. P., Zapata L. A., Rodríguez L. F., Pineda J. E., Vázquez-Semadeni E., 2010, ApJ, 725, 17
Garay G., Brooks K. J., Mardones D., Norris R. P., 2003, ApJ, 587, 739
Garay G. et al., 2007, A&A, 463, 217
Gibb E., Nummelin A., Irvine W. M., Whittet D. C. B., Bergman P., 2000, ApJ, 545, 309
Gooch R., 1996, in Jacoby G. H., Barnes J., eds, ASP Conf. Ser. Vol. 101, Astronomical Data Analysis Software and Systems V. Astron. Soc. Pac., San Francisco, p. 80
Hernández-Hernández V., Zapata L., Kurtz S., Garay G., 2014, ApJ, 786, 38
Hildebrand R. H., 1983, QJRAS, 24, 267
Hoffman I. M., 2012, ApJ, 759, 76
Jiménez-Serra I., Zhang Q., Viti S., Martín-Pintado J., de Wit W.-J., 2012, ApJ, 753, 34
Klaassen P. D., Wilson C. D., Keto E. R., Zhang Q., 2009, ApJ, 703, 1308
Kolesniková L., Tercero B., Cernicharo J., Alonso J. L., Daly A. M., Gordon B. P., Shipman S. T., 2014, ApJ, 784, L7
Krumholz M. R., Klein R. I., McKee C. F., Offner S. S. R., Cunningham A. J., 2009, Science, 323, 754

Kuiper R., Klahr H., Beuther H., Henning T., 2010, ApJ, 722, 1556

Linke R. A., Frerking M. A., Thaddeus P., 1979, ApJ, 234, L139

McMullin J. P., Waters B., Schiebel D., Young W., Golap K., 2007, in Shaw R. A., Hill F., Bell D. J., eds, ASP Conf. Ser. Vol. 376, Astronomical Data Analysis Software and Systems XVI. Astron. Soc. Pac., San Francisco, p. 127

Moscadelli L., Goddi C., 2014, A&A, 566, A150

Müller H. S. P., Schlöder F., Stutzki J., Winnewisser G., 2005, J. Mol. Struct., 742, 215

Naranjo-Romero R., Zapata L. A., Vázquez-Semadeni E., Takahashi S., Palau A., Schilke P., 2012, ApJ, 757, 58

Ossenkopf V., Henning T., 1994, A&A, 291, 943

Palau A. et al., 2011, ApJ, 743, L32

Palau A., Sánchez Contreras C., Sahai R., Sánchez-Monge Á., Rizzo J. R., 2013, MNRAS, 428, 1537

Panagia N., 1973, AJ, 78, 929

Peters T., Banerjee R., Klessen R. S., Mac Low M.-M., Galván-Madrid R., Keto E. R., 2010, ApJ, 711, 1017

Pickett H. M., Poynter R. L., Cohen E. A., Delitsky M. L., Pearson J. C., Müller H. S. P., 1998, J. Quant. Spectrosc. Radiat. Transfer, 60, 883

Qiu K., Zhang Q., Beuther H., Fallscheer C., 2012, ApJ, 756, 170

Rodríguez L. F., Moran J. M., Franco-Hernández R., Garay G., Brooks K. J., Mardones D., 2008, AJ, 135, 2370

Wang K.-S., van der Tak F. F. S., Hogerheijde M. R., 2012, A&A, 543, A22

Zapata L. A., Ho P. T. P., Schilke P., Rodríguez L. F., Menten K., Palau A., Garrod R. T., 2009, ApJ, 698, 1422

Zapata L. A., Tang Y.-W., Leurini S., 2010, ApJ, 725, 1091

Zapata L. A., Rodríguez-Garza C., Rodríguez L. F., Girart J. M., Chen H.-R., 2011, ApJ, 740, L19

Zinnecker H., Yorke H. W., 2007, ARA&A, 45, 481

This paper has been typeset from a TeX/LaTeX file prepared by the author.